# Conformational States and Dynamics of Rhodopsin in Micelles and Bilayers†

Ana Karin Kusnetzow, Christian Altenbach, and Wayne L. Hubbell*

*Jules Stein Eye Institute and Department of Chemistry and Biochemistry, University of California, Los Angeles, California 90095-7008*

*Received January 17, 2006; Revised Manuscript Received March 13, 2006*

ABSTRACT: Nitroxide sensors were placed in rhodopsin at sites 140, 227, 250, and 316 to monitor the dynamics and conformation of the receptor at the cytoplasmic surface in solutions of dodecyl maltoside (DM), digitonin, and phospholipid bilayers of two compositions. The EPR spectra reveal a remarkable similarity of rhodopsin structure and the activating conformational change in DM and bilayers, the hallmark of which is an outward tilt of transmembrane helix VI. This conformational change is blocked in solutions of digitonin, although changes in optical absorbance accompany activation, showing that absorbance and structural changes are not necessarily coupled. In DM and bilayers, the receptor is apparently in equilibrium between conformational substates whose populations are modulated by activation. Despite the general similarity in the two environments, the receptor conformations have increased flexibility in DM relative to bilayers. For the activated receptor in DM and bilayers, a pH-dependent conformational equilibrium is identified that may correspond to the optically characterized $\mathbf{MII_a}-\mathbf{MII_b}$ equilibrium. No specific effects of headgroup composition on receptor conformation in lipid bilayers were found.

Rhodopsin is a member of the large family of GPCR's[1] that act as input stages in signal transduction pathways (*1*). At this time, rhodopsin is the only GPCR with a known crystal structure (*2*−*5*), and it thus plays an important role as a structural paradigm for the entire family. Moreover, because rhodopsin is a chromoprotein activated by light, it has been possible to resolve intermediates along the activation pathway using UV−visible absorption properties in a way not possible with other receptors (*6*). Figure 1 shows some long-lived states of this receptor so identified that exist in the native membrane, where the asterisk indicates states capable of activation of the cognate G protein, transducin. The unliganded receptor, opsin (**Op**), has low basal activity (*7*). As for other GPCR's, constitutively active mutations and low pH activate the unliganded species (*8*, *9*). Covalent binding of the inverse agonist 11-*cis*-retinal to form rhodopsin (**R**) completely inactivates the receptor. Conversion of the bound 11-*cis*-retinal to the full agonist all-*trans*-retinal by absorption of a photon occurs on the time scale of femtoseconds (*10*) and initiates a temporal sequence of short-lived intermediates (*6*) that culminates within a few milliseconds in a pH-dependent equilibrium between species designated **MI** ($\lambda_{max} = 480$) and **MII** ($\lambda_{max} = 380$), of which

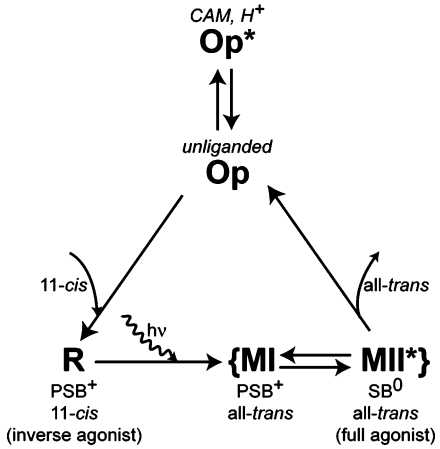


FIGURE 1: The inactive (**R**, **MI**, and **Op**) and active (**MII*** and **Op***) states of rhodopsin in native membranes. The retinal isomer and protonation state of the Schiff base linkage ($PSB^+$ = protonated and $SB^0$ = unprotonated) are noted under each species. The unliganded opsin (**Op**) is inactive but may be activated either by lowering the pH or by constitutively active mutations (CAM's).

**MII** is the physiologically active form of the receptor (*11*). Slow dissociation of the chromophore leads back to **Op**. Decay of **MII** to opsin also involves the parallel formation of another inactive species, **MIII** (not shown), believed to be a storage form of the receptor (*12*).

A central event in the formation of the activated **MII** species is the deprotonation of the Schiff base linkage between K296 and the retinal chromophore (*13*). In all species other than **MII**, the Schiff base is protonated, and a salt bridge is formed between the positive charge on the Schiff base located on TM7 and a counterion, either E113 (**R**) or E181 (**MI**) (*14*−*16*). The salt bridge is a key constraint that maintains the inactive form of the receptor, and its rupture is viewed as an obligatory step in activation (*8*, *17*).

† This work was supported by NIH Grant EY05216, the Jules Stein Professor Endowment, and a grant from the Ford Bundy and Anne Smith Bundy Foundation.

* To whom correspondence should be addressed. Telephone: (310) 206-8830. Fax: (310) 794-2144. E-mail: hubbellw@jsei.ucla.edu.

[1] Abbreviations: GPCR, G-protein-coupled receptor; SDSL, site-directed spin labeling; TM, transmembrane domain; **R**, inactive rhodopsin; **R***, activated rhodopsin; **Op**, opsin; **MI**, metarhodopsin I; **MII**, metarhodopsin II; POPC or PC, 1-palmitoyl-2-oleoyl-*sn*-glycero-3-phosphocholine; POPE or PE, 1-palmitoyl-2-oleoyl-*sn*-glycero-3-phosphoethanolamine; POPS or PS, 1-palmitoyl-2-oleoyl-*sn*-glycero-3-[phospho-L-serine]; DM, *n*-dodecyl *β*-D-maltopyranoside or dodecyl maltoside; MOMD, microscopic order/macroscopic disorder; WT, wild type.

10.1021/bi060101v CCC: $33.50 
Published on Web 04/07/2006

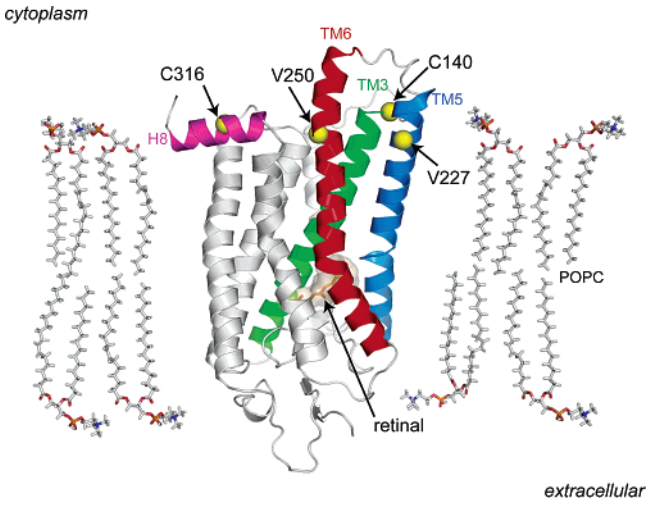


FIGURE 2: Ribbon model of rhodopsin in the inactive state (PDB ID 1GZM). Yellow spheres show the $C_\alpha$ atoms corresponding to sites where the R1 side chain was substituted in the present study (140, 227, 250, and 316). The location of the lipid bilayer relative to the protein was positioned according to SDSL and electron microscopy studies (see text). Helices are color coded as follows: TM3, green; TM5, blue; TM6, red; H8, magenta.

In micellar solutions of DM, the **MI** intermediate decays rapidly to produce pure **MII** (*18*, *19*). Arnis and Hofmann have kinetically resolved the existence of two isochromic forms of **MII** in DM, designated $\mathbf{MII_a}$ and $\mathbf{MII_b}$, in a pH-dependent equilibrium with an apparent p$K_a$ of 6.75 (*20*). It is presumed that $\mathbf{MII_a}$ and $\mathbf{MII_b}$ also exist in equilibrium with **MI** in the native membrane environment, and Stewart et al. provided early evidence for this presumption (*21*). For convenience in the following discussion, the designation **MII** will be used to refer to the sum of $\mathbf{MII_a}$ and $\mathbf{MII_b}$ unless a specific assignment to the subspecies is made, and **R*** will be used to refer to the collection of substates representing the photoactivated state. **R*** has also been characterized in solutions of digitonin, another micelle-forming amphiphile (*22*, *23*). A recent study showed that light activation of rhodopsin in digitonin micelles produces only **MI** and $\mathbf{MII_a}$ in a pH-independent equilibrium; the $\mathbf{MII_a} \rightarrow \mathbf{MII_b}$ transition is blocked (*23*). Thus, digitonin provides a tool for isolating the **MI** and $\mathbf{MII_a}$ species from $\mathbf{MII_b}$.

In addition to crystal structures for the inactive state **R** [Figure 2 (*2*−*5*)], a structure for **MI** has recently been determined by cryoelectron microscopy of two-dimensional crystals (*24*). The structure of **MI** is essentially identical to that of **R** at the cytoplasmic surface, where the major conformational change upon activation must occur to trigger binding of the G-protein. This supports the view built upon thermodynamic data that the activating conformational change occurs at the **MI** to **MII** transition (*20*).

A molecular description of opsin activation by the all-*trans*-retinal agonist, protons, and constitutively active mutations requires structural information on **MII**, **Op**, and **Op***. Undoubtedly, crystal structures will be obtained for activated forms of the molecule, perhaps in complex with the G-protein. However, it will also be necessary to obtain information on protein dynamic modes of these flexible structures in conformational equilibrium under native physiological conditions. For this purpose, spectroscopic approaches such as site-directed spin labeling (SDSL, *25*, *26*), FTIR (*27*), and NMR (*28*, *29*) are essential.

The structure and dynamics at the cytoplasmic face of **R** in DM solutions have been extensively studied by SDSL using singly spin-labeled sites at the cytoplasmic surface and pairs of labeled sites for distance measurements. The results of these experiments and a comparison with the first crystal structure of rhodopsin available at the time [PDB ID 1HZX (*2*)] have been reviewed (*26*). The structure at the cytoplasmic face inferred from SDSL data differs in two important respects from the 1HZX structure: (1) the TM5−TM6 interhelical loop, an important rhodopsin−transducin interaction sequence, was found by SDSL to be a dynamic helix−turn−helix motif rather than the irregular partial structure modeled from crystallographic data, and (2) the C-terminal sequence was found to be dynamically disordered by SDSL, whereas a structure, although poorly defined, was modeled from crystallographic data. A more recent crystal structure from a different space group [PDB ID 1GZM (*5*)] is in close agreement with the SDSL data, and that structure will be used here to interpret SDSL data.

The most direct structural information regarding light-activated conformational changes and the structure of the active **MII** state of rhodopsin has come from SDSL data obtained in DM solutions that revealed an outward displacement of TM6 at the cytoplasmic surface, with smaller motions of the rest of the helical bundle (reviewed in ref *26*). The rearrangement opens a cleft at the cytoplasmic surface of the molecule, presenting a new surface for interaction of the G-protein (*30*, *31*). Evidence supporting this motion and its generality among the members of the GPCR family has come from several experimental approaches (*1*, *32*, *33*).

All SDSL studies reported to date were done in DM solutions, and the question arises as to whether changes observed reflect those occurring in a lipid bilayer environment. The similarity in structures deduced by SDSL in solutions of DM and the 1GZM crystal structure, the ability of **R*** in DM to activate transducin (*22*), and the similar thermal stabilities of the protein in DM and native membranes (*34*, *35*) suggest that DM provides an adequate environment to stabilize both the inactive and active states of the receptor. Nevertheless, there are striking differences in photochemical behavior of rhodopsin in the native membranes and DM solutions. For example, the rate constant for decay of **MI** to **MII** is 2 orders of magnitude faster in DM than in membranes (*20*), and the equilibrium mixture of states in DM in the pH range of 6−8 contains only $\mathbf{MII_a}$ and $\mathbf{MII_b}$ as mentioned above, whereas **MI** is also present in native membranes. Studies of rhodopsin structural changes upon activation have also been carried out in digitonin solutions, and similar questions regarding the degree of conformational perturbation by the detergent arise.

The purpose of the present study is to compare the conformation and dynamics of **R** and **R*** in DM and digitonin and reconstituted in phospholipid bilayers and, where possible, to correlate conformation with the presence of the **MI**, $\mathbf{MII_a}$, and $\mathbf{MII_b}$ intermediates identified by UV−vis absorbance properties and/or kinetic methods. The nitroxide side chain R1 (Figure 3) was introduced at either site 140, 227, 250, or 316 to act as a sensor to monitor the conformation and dynamics of the helical bundle at the cytoplasmic surface. The R1 side chain has previously been employed at these sites to monitor conformational changes

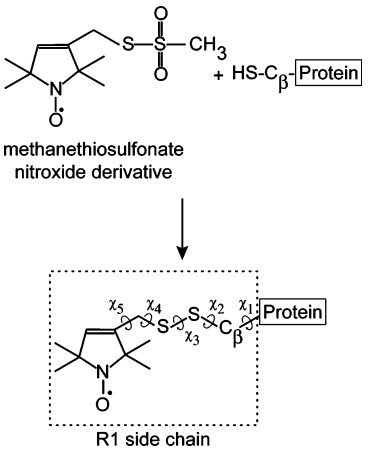


FIGURE 3: Reaction of the methanethiosulfonate spin-labeling reagent with cysteine to generate the nitroxide side chain, R1. The dihedral angles ($X_1-X_5$) are defined.

in DM due to constitutively active mutations of rhodopsin in DM (*17*, *36*). The location of each of these side chains in the 1GZM structure is shown in Figure 2, which includes phospholipids modeled at positions consistent with SDSL (*26*) and cryoelectron microscopy data from 2D crystals (*37*). In the present study, preferred rotamers of R1 are used to model the side chain in the 1GZM structure, and the models serve as a basis for interpretation of the corresponding EPR spectra in terms of local protein structure and dynamics in both detergent solutions and lipid bilayers.

## METHODS

*Construction and Expression of the Mutant Rhodopsin Genes.* The expression construct, pMT4-Rho, containing the base mutant $\phi$ (C140S/C316S) has been described previously (*19*). Four individual cysteine mutations (250C, 227C, 140C, and 316C) were introduced in the base mutant $\phi$, one at a time, according to published procedures (*38*). Two methods for the transient transfection of the construct in mammalian COS1 cells were employed: the DEAE-dextran-mediated method (*38*) and the cationic liposome-mediated method (*39*). The liposome-mediated method was modified: LipofectAMINE (Invitrogen Life Technologies Co.) was substituted by 50 $\mu$L of Maxfect (MediaTech, Inc.) and 15 $\mu$g of plasmid DNA per plate was used.

*Purification of the Rhodopsin Mutants and Derivatization with Spin Labels.* Recombinant rhodopsin in intact cells was regenerated with 11-*cis*-retinal (National Eye Institute of the National Institutes of Health), solubilized in DM (Anatrace, Inc.), purified using a 1D4 monoclonal antibody (University of British Columbia) immobilized on Sepharose (*38*), and derivatized with the nitroxide methanethiosulfonate reagent (Figure 3) while bound to the 1D4 column (*19*). The protein was eluted from the column in the appropriate detergent [0.4 mM DM, 34 mM *n*-octyl $\beta$-D-glucopyranoside (Alexis Biochemicals), or 0.16 mM digitonin (Acros Organics)] containing 100 $\mu$M peptide corresponding to the last nine C-terminal amino acids of rhodopsin (American Peptide Co., Inc.). Fractions containing rhodopsin were collected and concentrated to 30−50 $\mu$M. The final detergent concentration was estimated at ∼12−15 mM DM and ∼5−7 mM digitonin.

*Reconstitution of Rhodopsin in Lipids.* POPC, POPE, and POPS (Avanti Polar Lipids, Inc.) in the desired molar ratio and buffer were extruded using a LipsoFast membrane extruder (Avestin, Inc.) with a membrane pore diameter of 200 nm. Asymmetric rhodopsin proteoliposomes, with the extracellular side facing the interior of the vesicle, were prepared from the extruded lipids and spin-labeled rhodopsin in *n*-octyl $\beta$-D-glucopyranoside as described (*40*−*42*). Detergent was removed by extensive dialysis, and proteoliposomes were separated from protein-free liposomes by sucrose density ultracentrifugation (*43*). The lipid to protein molar ratio was calculated from the protein and lipid concentrations determined by Bradford (Pierce Biotechnology) and phosphorus assays (*44*), respectively. Typical lipid to protein ratios were ∼300−400 lipids per rhodopsin. The lipid composition of the proteoliposomes was verified by TLC (*45*). The diameter of the proteoliposomes was determined to be ∼200 nm by particle light scattering (Particle Sizing Systems, Inc.). Reconstituted samples were used within 24 h of preparation, before significant aggregation of the proteoliposomes occurred.

*Optical Spectroscopy.* Aliquots of the rhodopsin samples used in EPR experiments were diluted in the appropriate buffer to a final $A_{500}$ of ∼0.2−0.5. UV−vis spectra were collected on a Cary 50 (Varian, Inc.) equipped with a temperature-controlled sample holder. Samples were equilibrated at 20 °C in the dark for 30 min before the spectrum of **R** was collected, followed by in situ illumination for 30 s ($\lambda$ > 514 nm) and collection of the **R*** spectrum. The absence of free retinal after 20 min was verified by lowering the pH to 1.8; in all cases, the absorbance maximum shifted to 440 nm, characteristic of a protonated retinyl Schiff base (*46*). The light minus dark state difference spectrum was calculated to circumvent the scattering problems in the reconstituted samples. To determine the amount of **MI** and **MII** present, the difference spectra were fit, as a weighted sum of reference spectra of the pure components (**R**, **MI**, and **MII**), using a program written in LabVIEW (National Instruments). The results of the general *k*-dimensional linear least-squares fits were normalized so that the **R** component had an amplitude of −1 (complete bleaching). The sum of the remaining components was always 1 ± 0.08. The reference spectrum for **R** at 25 °C was obtained from WT (from rod outer segments) purified in DM, and that for **MII** was obtained upon illumination of **R**. The **MI** reference spectrum was obtained at 0 °C upon illumination of WT (from rod outer segments) purified in digitonin. An example of the analysis is shown in Figure 4 for the difference spectra of 140R1 in DM at pH 6 and 316R1 in PC:PE:PS bilayers at pH 6.

*EPR Spectroscopy. (A) Continuous Wave EPR Spectroscopy.* EPR spectra of samples were measured in a Bruker ELEXSYS 580 fitted with a High Sensitivity resonator in small volume aqueous flat cells (Wilmad Glass Co. Inc.). Spectra were recorded at 100 G scan widths over 30 s with an incident microwave power of 20 mW and modulation amplitude of 4 G. This modulation optimized the signal to noise ratio and was verified to produce minimal spectral distortions. Samples were equilibrated in the dark at 20 or 35 °C for 30 min before the **R** spectrum was collected, followed by 30 s of illumination in situ ($\lambda$ > 514 nm) and the collection of the spectrum for **R***. Typically, nine scans

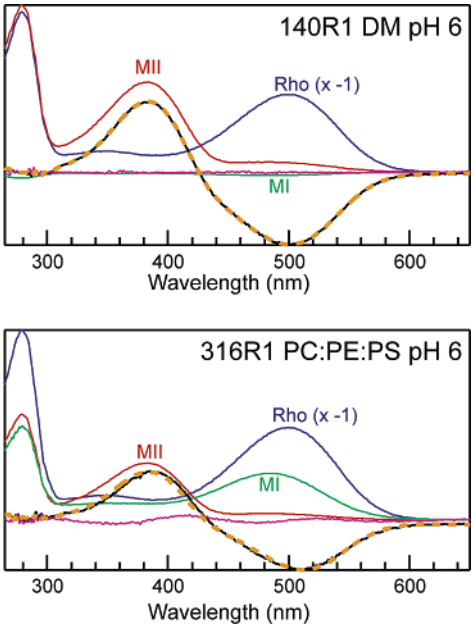


FIGURE 4: Example of light − dark difference spectra (black trace) of the labeled rhodopsin mutants in DM and PC:PE:PS bilayers at pH 6 and 20 °C. The fit to the difference spectrum (dashed orange trace) and the contributions of **R** (blue trace), **MI** (green trace), and **MII** (red trace) to the difference spectrum are also shown. The magenta trace is the residual from the fit.

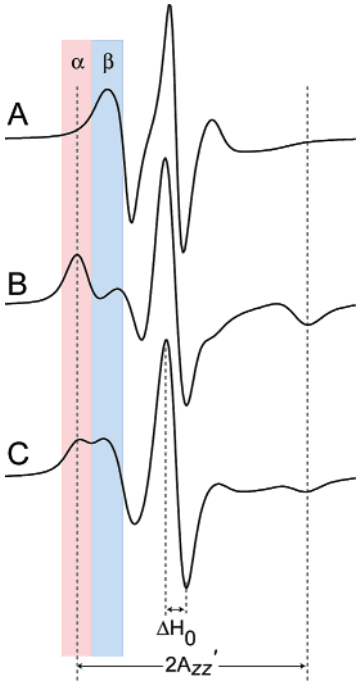


FIGURE 5: Simulated EPR spectra and semiempirical parameters used to infer nitroxide mobility for different dynamic modes. (A) Rapid anisotropic motion. (B) Slow isotropic motion. (C) A complex state corresponding to a weighted sum of (A) and (B). The central line width ($\Delta H_0$) and splitting of resolved hyperfine extrema ($2A_{zz}'$) are identified. Spectral intensity in regions α and $\beta$ identifies relatively immobile and mobile components, respectively.

were signal-averaged per spectrum, and the total collection time did not exceed 5 min. For rhodopsin in bilayers, the EPR spectra are time-dependent due to the decay of **MI**/**MII** to **Op** and/or **MIII**. On the basis of the decay rate in membranes at 20 °C (*12*), it can be estimated that the signal-averaged EPR spectrum obtained over a 5 min period represents that for bilayers containing no more than 10% of **Op** and/or **MIII**.

*(B) Interpretation of EPR Spectra in Terms of Nitroxide Motion*. As shown in Figure 2, all of the R1 sensors in the present studies are in helices. At surface sites, where the nitroxide ring does not have interactions with the surrounding protein, the internal motion of R1 due to torsional oscillations about the bonds of the side chain can generally be described in terms of an order parameter ($S$), measuring the amplitude or order of motion, and a correlation time ($\tau$), the inverse of which measures the rate of motion (*47*). This internal motion is modulated by fluctuations of the backbone, giving rise to motions with $S \leq 0.5$ and $\tau$ in the range of 1−3 ns. An example of a weakly ordered state of R1 with $S = 0.2$ and $\tau = 2$ ns is shown by the spectrum in Figure 5A simulated according to the MOMD model of Freed and co-workers (*48*). For motions of this kind, changes in the central line width ($\Delta H_0$) serve as a qualitative measure of changes in rate of motion, with increasing line width corresponding to a decrease in rate (*47*). Interactions of the nitroxide ring with the protein lead to various degrees of immobilization, due either to an increase in order, a decrease in $\tau$, or both. An example of a relatively immobilized state with isotropic motion ($S = 0$) and $\tau = 50$ ns is shown by the simulated spectrum in Figure 5B. Such a spectrum would arise, for example, for a nitroxide immobilized with respect to the protein and thus having a correlation time determined by protein rotary diffusion. For immobilized states with well-resolved hyperfine extrema, changes in the overall splitting between the extrema ($2A_{zz}'$, Figure 2B) provide a measure of changes in mobility; decreases or increases in $2A_{zz}'$ reflect an increase or decrease in mobility, respectively (*49*).

Often, the EPR spectrum of R1 reflects multiple dynamic states of the side chain, arising either from two rotamers of the side chain, each having different degrees of interaction with the environment (*50*), or from two states of the protein. An example of such a complex spectrum is shown in Figure 5C, which is a weighted sum of the spectra in Figure 5A,B. Such spectra are typical of those for R1 in rhodopsin. In these cases, changes in $2A_{zz}'$ still reflect changes in mobility of the more immobilized state. For complex spectra arising from states of widely different mobility, as encountered here and illustrated in Figure 5C, the more immobile component dominates spectral intensity in the region labeled α. Likewise, the more mobile component dominates spectral intensity in the region labeled $\beta$. Changes in intensity in these two regions will be taken to reflect corresponding changes in the population or dynamics of these two states.

Fitting of single- or multiple-component EPR spectra to the MOMD model of Freed and co-workers is a method of extracting quantitative information on orders and rates of motion for R1 in proteins (*48*, *49*, *51*). This model permits the simulation of spectra arising from an isotropic distribution of nitroxides undergoing anisotropic motion, which corresponds to the physical situation of a spin-labeled protein in which the rotary diffusion of the protein is slow compared to the internal motion of R1. In the context of the MOMD model, the motion of the nitroxide in R1 on solvent-exposed sites can often be described by a single order parameter, $S$, and an effective correlation time, $\tau_c$ (*47*, *52*, *53*).

For the important mutant 250R1, experimental EPR spectra were fit to a two-component MOMD model to extract information on the dynamics of the populations. Values for the **A** and **g** tensors used in simulations of strongly immobilized states were determined by fitting spectra of 250R1 obtained from dark-adapted rhodopsin in the absence of motion at −50 °C. The values are $A_{xx} = 5.1$, $A_{yy} = 4.6$, $A_{zz} = 35.5$, $g_{xx} = 2.0082$, $g_{yy} = 2.0065$, and $g_{zz} = 2.0022$. To constrain the number of parameters, the immobilized state is taken to have isotropic motion. It is further assumed that the more mobile state in two-component spectra is exposed to water, and **A** and **g** tensor values previously reported for R1 in an aqueous environment were employed, namely, $A_{xx} = 6.2$, $A_{yy} = 5.9$, $A_{zz} = 37.0$, $g_{xx} = 2.0078$, $g_{yy} = 2.0058$, and $g_{zz} = 2.0022$ (*47*, *51*). The models presented in Results and the good fits to the data justify these assumptions. Fitting procedures followed those previously described (*47*, *53*).

*Modeling of the Nitroxide Side Chain in Rhodopsin.* The R1 side chain was modeled at residues 140, 227, 250, or 316 in the 1GZM rhodopsin structure using DS Viewer Pro (Accelrys, Inc.), and all molecular graphics were generated using the PyMOL Molecular Graphic System (DeLano Scientific, LLC). The R1 rotamers about $X_1$ and $X_2$ (Figure 3) modeled were those commonly found in crystal structures of R1 at helical sites in T4 lysozyme (T4L), namely, {*m*, *m*}, {*t*, *p*}, and {*t*, *m*} (*50*; Fleissner, Cascio, Sawaya, Hideg, and Hubbell, unpublished results; Guo, Cascio, and Hubbell, unpublished results). The rotamer notation is that of Richardson et al. (*54*), where $m = -60 \pm 10$, $p = +60 \pm 10$, and $t = 180 \pm 10$. Each structure was optimized by variation of the $X_4$ and $X_5$ dihedrals without moving native side chains. Allowed rotamers were determined by manual changes in dihedrals of R1, while avoiding overlap of the nitroxide side chain with other atoms.

## RESULTS

*Comparison of **R** and **R*** in DM and Phospholipid Bilayers.* EPR spectra of 140R1, 227R1, 250R1, and 316R1 are presented in Figures 6−9 for **R** and **R*** at pH 6 in solutions of DM and reconstituted in POPC:POPE:POPS bilayers having a composition approximating that of the native disk membrane (5:4:1 mol ratio) (*55*). In each case, data were also collected for the spin-labeled proteins reconstituted in pure POPC. Within experimental error, the corresponding EPR spectra were identical to those shown for POPC:POPE:POPS mixed bilayers.

In DM at 20 °C, **R*** for each spin-labeled mutant contained 100% **MII** immediately after photoactivation, as determined from the 380 nm absorbance, consistent with published data on WT rhodopsin (*19*, *35*). All EPR spectra of **R*** in DM (12−15 mM) were time-independent for at least 2 h.

In phospholipid bilayers both **MI** and **MII** are present. The relative amounts were determined within a few minutes after complete photolysis of rhodopsin as described in Methods, and the values are provided below in terms of the apparent (pH-dependent) equilibrium constant $K = \mathbf{MII}/\mathbf{MI}$. The **MI** and **MII** intermediates (monitored optically) decay slowly to opsin or a mixture of opsin and **MIII** (*12*), and the EPR spectra in the light-activated state are also time-dependent. The EPR spectra reported here were acquired within a short interval following activation and correspond primarily to the initial mixture of **MI** and **MII** (see Methods). The time-dependent changes in EPR spectra accompanying the decay of **MI** and **MII** will be reported elsewhere. The following sections consider the results for each spin-labeled mutant.

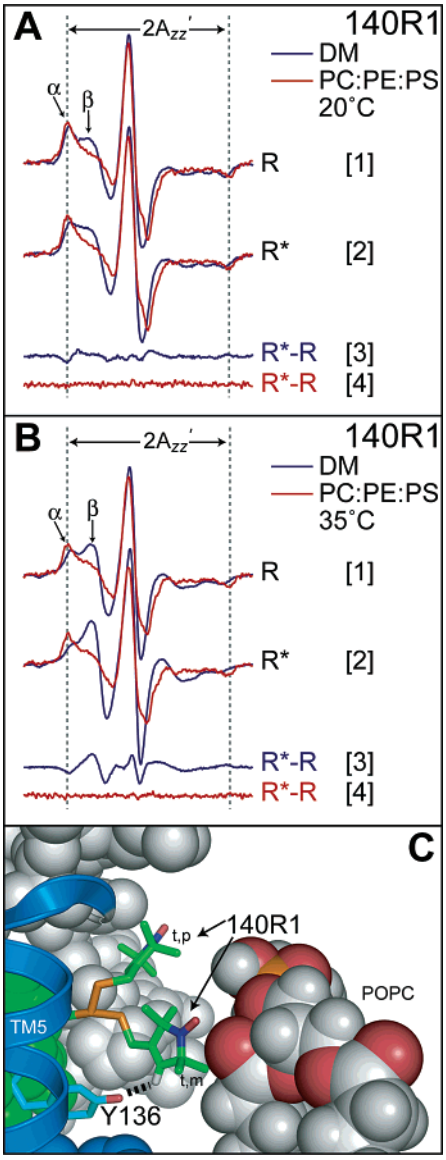


FIGURE 6: EPR spectra of rhodopsin 140R1 in DM and PC:PE:PS bilayers at pH 6 and molecular models of the side chain. (A) Spectra for the indicated samples at 20 °C (parts [1] and [2]). (B) Spectra for the indicated samples at 35 °C (parts [1] and [2]). In (A) and (B), **R*** − **R** difference spectra are shown to highlight the changes upon light activation (parts [3] and [4]). (C) Models of 140R1 in the 1GZM rhodopsin crystal structure. TM3 is shown in green, a portion of TM5 is shown as a blue ribbon, and a nearby phospholipid is modeled.

*(A) 140R1.* Residue 140 is located near the contact face of TM3 and TM5 in the headgroup region of the lipid bilayer (Figure 2). Figure 6A[1] shows a comparison of the EPR spectra for 140R1 **R** at 20 °C in DM and PC:PE:PS bilayers. In DM, the spectrum has two dominant components, reflecting relatively immobilized (α) and mobile (*β*) states of the side chain. In PC:PE:PS bilayers, there is strong overall immobilization of the nitroxide relative to DM revealed by an increase in the splitting of the outer hyperfine extrema ($2A_{zz}'$), an increase in $\Delta H_0$, and a decrease in the spectral intensity in the *β* region of the spectrum.

Figure 6A[2] compares the corresponding spectra for **R***. The small change upon light activation in DM previously reported (*19*) is reproduced, as shown by the **R*** − **R** difference spectrum of Figure 6A[3], and reveals a shift toward a more mobile population. In bilayers, 140R1 **R*** remains immobilized, and the change upon activation is entirely lost (Figure 6A[4]), although the 140R1 **R*** population contains both **MI** and **MII** with an equilibrium constant $K = 1.5$, consistent with that for the WT protein reconstituted in a similar lipid mixture at pH 6 (*56*, *57*).

The strong immobilization of the 140R1 side chain in bilayers could mask small changes upon activation; therefore, studies were also carried out at 35 °C, and the corresponding spectra are shown in Figure 6B. The spectral line widths of 140R1 **R** and **R*** in DM are decreased due to increased molecular motion, and the change upon activation is similar in shape but much larger than at 20 °C (Figure 6B[1]−[3]). In PC:PE:PS bilayers, the nitroxide remains immobilized, and there is no change upon activation (Figure 6B[4]). The spectra of 140R1 in both **R** and **R*** are remarkably temperature-independent in the lipid bilayers.

One interesting possibility for the origin of the two dynamic modes of 140R1 is the presence of two protein conformations in equilibrium, but it is also possible that the two modes arise from two rotamers of the side chain in which one makes immobilizing interactions with the protein (*50*). The data do not allow these possibilities to be distinguished, so R1 was modeled in **R** to gain additional insight. As shown in Figure 6C, two commonly observed rotamers of R1, {*t*, *m*} and {*t*, *p*}, can be modeled at 140 in the 1GZM structure. In the {*t*, *m*} rotamer, the nitroxide ring can be positioned close to Y136 in a geometry that favors a CH−O hydrogen bond of the kind observed in crystal structures of R1 in T4 lysozyme (*50*). This interaction constrains the nitroxide and, together with other local interactions, could account for the more immobilized component in the spectra of 140R1 rhodopsin in DM. The mobile component could arise from the {*t*, *p*} rotamer, where the ring is positioned away from Y136 and free to move via torsional oscillations about the $X_4$ and $X_5$ dihedrals. Thus, modeling indicates that the two dynamic modes of 140R1 **R** and **R*** in DM could be due to a simple rotameric equilibrium but cannot eliminate the possibility of conformational heterogeneity of the protein.

The striking immobilization of 140R1 for both **R** and **R*** in bilayers may signal a local change in conformation relative to that in DM. However, another possibility is suggested by the model of Figure 6C. For example, 140R1 projects directly into the highly ordered headgroup domain of the bilayer, an environment which has been found to strongly damp the motion of the R1 side chain on membrane-associated annexin (*58*). In addition, if a CH−O H-bond is in fact formed, it may be strengthened in the partially hydrophobic environment of the headgroup region, leading to stabilization of the {*t*, *m*} state and immobilization. In either case, immobilization of 140R1 leads to loss of sensitivity to structural changes upon activation. Finally, immobilization of 140R1 could result from formation of a rhodopsin dimer in which 140R1 is at the dimer interface. The existence of a rhodopsin dimer remains controversial (*59*), but one model for a putative dimer has been proposed (*60*−*62*). In this model 140R1 is not in the dimer interface, and the presence of the dimer in the reconstituted membranes could not account for the observed immobilization of 140R1.

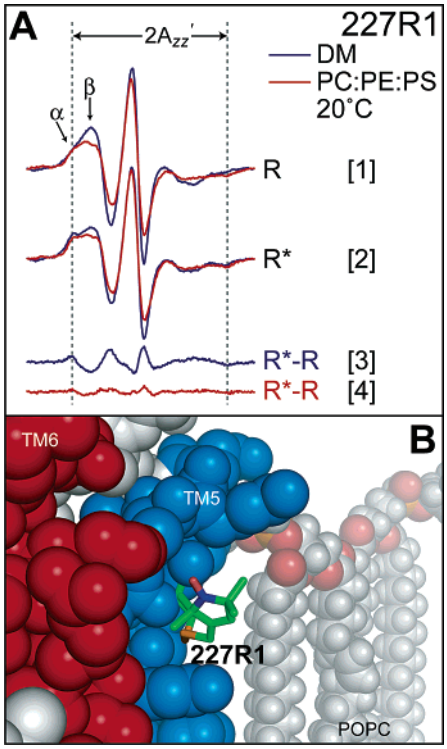


FIGURE 7: EPR spectra of rhodopsin 227R1 in DM and in PC:PE:PS bilayers at pH 6, 20 °C, and a molecular model of the side chain. (A) Spectra for the indicated samples (parts [1] and [2]). **R*** − **R** difference spectra are shown to highlight the changes upon light activation (parts [3] and [4]). (B) A model of one rotamer of 227R1in the 1GZM rhodopsin crystal structure. TM5 is shown in blue, and nearby phospholipids are modeled.

*(B) 227R1.* Residue 227 is located in TM5, directly facing the hydrocarbon chains of the bilayer below the headgroup region (Figure 2). Figure 7A[1] compares the spectra of 227R1 **R** in DM and in lipid bilayers. In DM, the spectrum reflects a dominant component with a relatively high degree of mobility characteristic of an R1 residue on the aqueous-exposed surface of an α-helix in soluble proteins (*47*), but with broader features likely due to a heterogeneous and more viscous environment of the micelle interior compared to water. In PC:PE:PS bilayers, the spectrum reveals an overall decrease in mobility relative to that in DM, as evidenced by an increase in $\Delta H_0$ [$\Delta(\Delta H_0) = 0.6$ G], a corresponding decrease in spectral amplitude in the normalized spectra, and the appearance of a component with partially resolved high- and low-field extrema at the positions of the vertical dotted lines. The decrease in mobility is likely due in part to the increased molecular order of the bilayer environment near the headgroup region.

Figure 7A[2] compares the spectra of 227R1 **R*** in DM and lipid bilayers. In DM, the salient difference between **R** and **R*** is the appearance of a strongly immobilized component at the expense of more mobile states, as shown by the positive and negative features in the **R*** − **R** difference spectrum in the α and *β* regions, respectively (Figure 7A[3]). This previously reported light-dependent change was interpreted to reflect new immobilizing interactions of 227R1 with groups in TM6 as it moves outward (*63*).

In lipid bilayers, the overall mobility in **R*** is again decreased relative to DM, but the light-dependent change is retained, although of smaller magnitude (Figure 7A[3],[4]). In the bilayers, 227R1 **R*** contains both **MI** and **MII** ($K$ = 0.7). The smaller magnitude of light-dependent change in the bilayers may be due in part to the presence of **MI**, absent in DM, which is expected to have a conformation similar to **R** (*64*).

For reference, Figure 7B shows the 227R1 side chain modeled in the 1GZM structure. In the unrestrictive environment at this site, all three common rotamers can be modeled without steric clashes. In each, the nitroxide has an environment dominated by direct contact with the hydrocarbon chains of either the micelle or the bilayer. The multiple rotamers and the freedom of motion about $X_4$ and $X_5$ are consistent with a dominant component of relatively high mobility observed at this site in **R**.

*(C) 250R1*. Residue 250 lies in TM6, projecting into the interior of the helix bundle (Figure 2). Unlike 140R1 and 227R1, 250R1 does not have contacts with the lipid or micelle environment, and the motion reflects only interactions with the protein. Figure 8A[1] compares the EPR spectra of 250R1 for **R** in DM and in lipid bilayers of PC:PE:PS. In both environments the spectra are dominated by a strongly immobilized state, but spectral intensity in the $\beta$ region indicates the presence of a more mobile state as well (compare with Figure 5B). The values of $\Delta H_0$ and $2A_{zz}'$ in lipid bilayers are larger than those for DM, indicating a lower mobility for R1 in bilayers.

Figure 8A[2] compares the spectra of **R*** in DM and lipid bilayers, where the overall similarity of the spectra is evident. The dramatic line shape change upon activation, in both DM and lipid bilayers, indicates a shift in the R1 population toward a more mobile state (Figure 8A[3],[4]). In solutions of DM, this was previously interpreted in terms of an outward movement of TM6 that removes constraints on the motion of 250R1 (*30*, *63*), a hallmark of the receptor activation. The fact that this activating conformational change and the coupled change at 227R1 are preserved in lipid bilayers is an important conclusion of this study.

To quantitatively characterize the motion for R1 at this important site, the spectra were fit to a two-component MOMD model as described in Methods. The fits, shown as dotted traces overlaid on the experimental spectra in Figure 8B, provide values for the order parameters ($S$), effective correlation times ($\tau_c$), and fractional occupancies ($f$) for the components (Table 1).

For **R** in DM, $\tau_c$ = 77 ns for the more immobile state corresponding to the rotational diffusion of a spherical object of radius 42 Å, the same as the hydrodynamic radius determined for **R** in DM micelles by gel permeation chromatography (*65*). This indicates that the nitroxide population that gives rise to this component has a motion determined by the overall rotational diffusion of the **R**−DM micellar complex. For **R** in PC:PE:PS bilayers, $\tau_c \approx 200$ ns for the immobile component. The rotational diffusion of **R** in bilayers is slow on the X-band EPR time scale ($\tau_c \sim 10-20$ $\mu$s; *66*, *67*), and the correlation time for the nitroxide apparently represents slow fluctuation of the nitroxide with respect to the protein.

In both DM and bilayers, the mobile component has weak ordering ($S \sim 0.3$) and fast motion ($\tau_c \sim 3$ ns), corresponding to an R1 side chain having little tertiary interaction with the protein (*68*). A difference between 250R1 in DM and bilayers lies in the significantly larger proportion of the mobile component in DM.

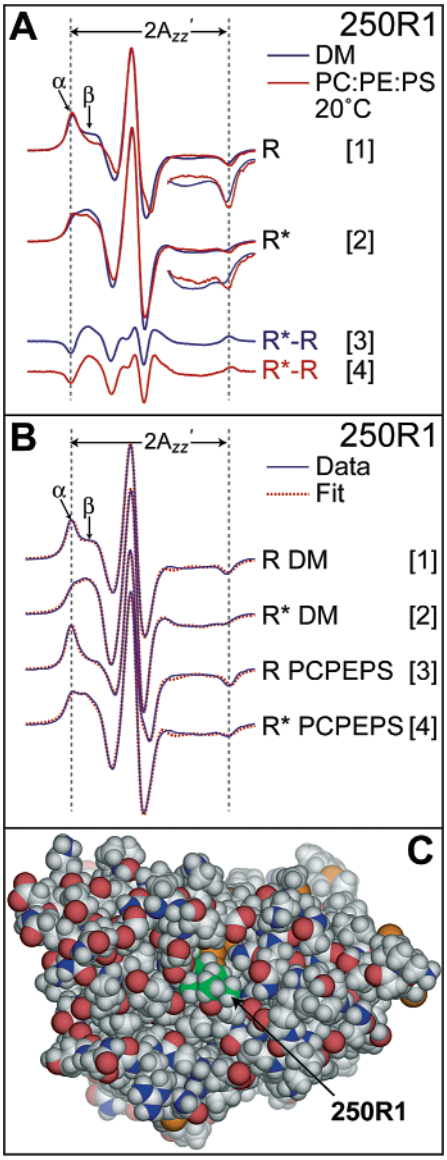


FIGURE 8: Experimental and simulated EPR spectra of rhodopsin 250R1 in DM and PC:PE:PS bilayers at pH 6, 20 °C, and a molecular model of the side chain. (A) Experimental spectra for the indicated samples (parts [1] and [2]). **R*** − **R** difference spectra are shown to highlight the changes upon light activation (parts [3] and [4]). (B) Simulated spectra (red dotted traces) of 250R1 **R** and **R*** in DM and bilayers are shown superimposed on the corresponding experimental spectra (solid blue traces). (C) Space-filling model of 250R1 (carbon atoms shown in green) in the 1GZM rhodopsin crystal structure viewed from the cytoplasmic surface.

Table 1

| host system | receptor state | immobile component $\tau_c$ (ns) | immobile component $f^a$ | mobile component $\tau_c$ (ns) | mobile component $S$ | mobile component $f^a$ |
|---|---|---|---|---|---|---|
| DM | **R** | 77 | 0.43 | 3.4 | 0.31 | 0.57 |
| | **R*** | 26 | 0.29 | 3.1 | 0.26 | 0.71 |
| PC:PE:PS | **R** | ≈200 | 0.56 | 3.4 | 0.33 | 0.44 |
| | **R*** | 83 | 0.42 | 3.0 | 0.30 | 0.58 |

[a] $f$: the fractional population.

MOMD fits to the **R*** spectra in DM and bilayers again reveal the presence of both relatively immobile and mobile components, but with an increased proportion of the mobile state relative to **R**. However, in both environments the more immobile component has a significantly shorter $\tau_c$ relative to **R**.

In DM, 250R1 **R*** is pure **MII**, while in lipid bilayers **MI** is also present, but at relatively low levels ($K = 4$). The larger value of $K$ relative to WT under similar conditions ($K = 1.5$) suggests a mild perturbation of the equilibrium by 250R1 favoring **MII**.

Figure 8C shows a model of the R1 side chain at site 250 in the 1GZM rhodopsin structure looking down at the cytoplasmic surface. Due to the constrained environment around 250, only a single rotamer can be built without atomic overlaps or altering the structure of the protein. This unusual rotamer is $\{m, t\}$, the same as that observed in the crystal structure of T4L 75R1 where the environment is similarly constrained, and is not one of the "relaxed" conformations of the side chain seen at solvent-exposed helix surface sites (*50*). The nitroxide ring resides in an existing pocket in **R**, making numerous van der Waals contacts with neighboring atoms that would strongly constrain its motion, accounting for the component in the EPR spectrum corresponding to an immobilized state.

Considering that no other rotamer of the nitroxide can be modeled in **R** that would give rise to a mobile state of R1, it is likely that the more mobile component represents a second conformational substate of the protein in equilibrium with that corresponding to the crystal structure. This interpretation is strengthened by the fact that this component is reduced in PC:PE:PS bilayers, although the nitroxide itself is well removed from direct contact with the bilayer environment. Models for the putative substates of the protein in both **R** and **R*** will be considered below in the Discussion.

*(D) 316R1.* Residue 316 resides on the solvent-exposed surface of the short helix 8 (H8) that lies perpendicular to the TM helical bundle (Figure 2). Like 250R1, the side chain is not expected to have direct contacts with the micellar or bilayer environment. Figure 9A[1] compares the EPR spectra of 316R1 for **R** in DM and in PC:PE:PS bilayers. As for 140R1 and 250R1, the spectra each reveal two well-resolved components corresponding to relatively immobilized and mobile states of R1, but with a different population ratio, reflecting a local structural difference in DM and lipid bilayers around 316. As discussed above for 140R1, the two states of R1 could arise from conformational heterogeneity of either R1 or the protein, and these possibilities cannot be distinguished from the spectra alone.

A similar difference between DM and lipid bilayers is seen in **R***, although the effect is smaller (Figure 9[2]). The change upon activation in DM corresponds to a small shift in the population toward the immobile state, as reported earlier (Figure 9[3]). The same change with larger amplitude is observed in bilayers (Figure 9[4]), due primarily to the difference in the **R** state spectra. In DM, 316R1 **R*** is pure **MII**; in lipid bilayers, **MI** is also present ($K = 1.5$ at pH 6, the same as for the WT protein).

A model of the R1 side chain at 316 is shown in Figure 9B. Due to the crowded environment around this site, only the $\{m, m\}$ rotamer can be built, but both $\pm 90$ configurations of $X_3$ (the disulfide) can be accommodated. In one ($X_3 = -90$, shown in Figure 9B), multiple contacts of the R1 side chain with residues H65 and K67 in the TM1−TM2 loop are made, a situation which could give rise to the immobilized state. In the other ($X_3 = +90$, not shown), the ring projects outward over the H8 helix where no obvious interactions of the ring are possible, allowing freedom of motion about $X_4$ and $X_5$. Due to the slow interconversion rate about $X_3$ on the EPR time scale, this situation could give rise to resolved mobility states of R1. In accounting for the two dynamic states of 316R1, it must also be considered that the C-terminal tail of the molecule, not resolved in the crystal structure, could lie over the H8 helix and make contacts with 316R1.

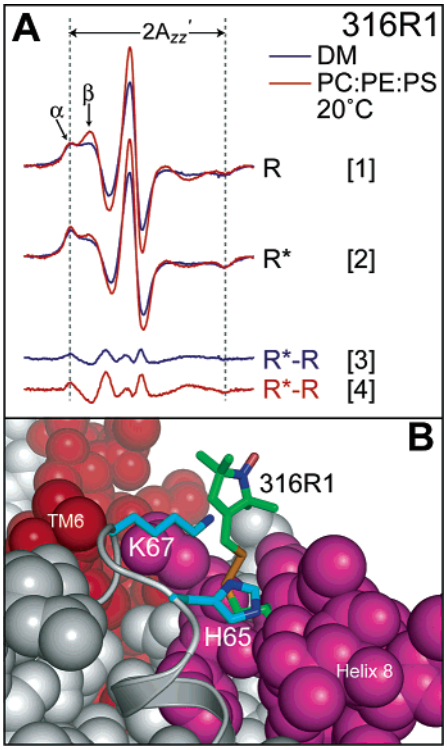


FIGURE 9: EPR spectra of 316R1 in DM and PC:PE:PS bilayers at pH 6, 20 °C, and a molecular model of the side chain. (A) Spectra of the indicated samples (parts [1] and [2]). **R*** − **R** difference spectra are shown to highlight the changes upon light activation (parts [3] and [4]). (B) A model of 316R1 in the 1GZM rhodopsin crystal structure. Helix H8 is shown in magenta. For clarity, the cytoplasmic end of TM1 and the loop between TM1 and TM2 are shown as gray ribbons.

*pH Dependence of **R** and **R*** Conformations in DM and Phospholipid Bilayers.* The dependence of structure on pH is of particular importance for rhodopsin and other GPCR's because the population of the active conformation is directly modulated by pH. Changes in pH can produce changes in the motion of R1 due to local or global structural effects. Local effects arise from protonation changes of residues in the immediate environment without consequences for the overall protein structure and complicate interpretation of spectral changes in terms of protein conformational changes. Residues 227R1 and 316R1 were found to show significant spectral changes with pH even in **R** (data not shown). While these could represent global conformational transitions, the presence of nearby basic residues could have local effects. In the case of 227R1, nearby lysine residues K231 and K248 reside at the bilayer−water interface, where the $pK_a$ could be shifted downward into the pH 6−8 range. For 316R1,

the nitroxide ring is in close proximity to H65, which titrates in the relevant pH range. Thus, 227R1 and 316R1 were not considered for further investigation of pH-dependent conformational changes. 140R1 was not employed because light-dependent changes are completely masked in lipid bilayers. On the other hand, the **R** spectrum of 250R1 shows no pH dependence in the range 6−8, and the dependence of R1 dynamics on protein conformation makes it a suitable choice for exploring the effect of pH.

Parts [1] and [2] of Figure 11A show the effects of pH on the EPR spectra for both **R** and **R*** in DM, where only **MII** is populated. There is little effect of pH on **R**, but a small reversible pH change is noted in **R***. The insets are provided to clearly reveal the changes in the low- and high-field regions, which show that high pH shifts the population toward the more immobilized state, i.e., toward a state more closely resembling the **R** state. Consequently, the **R*** − **R** difference spectra (Figure 10A[3],[4]) show a larger change at pH 6 compared to pH 8. These results are compatible with a pH-dependent equilibrium between conformational substates for the activated receptor in the detergent micelle. Because $\mathbf{MII_a}$ and $\mathbf{MII_b}$ in DM titrate with a p$K_a$ of 6.75, the substates are tentatively identified with these intermediates. In this case, the spectra of 250R1 at pH 6 and 8 largely reflect the structures of $\mathbf{MII_b}$ and $\mathbf{MII_a}$, respectively. For reference, Figure 10B compares the spectrum of **R** with the spectra assigned to these species.

The corresponding data for 250R1 in POPC:POPE:POPS in Figure 10C show qualitatively similar results, suggesting that $\mathbf{MII_a}$ and $\mathbf{MII_b}$ states may exist in the bilayer as well as in the DM environment. The EPR spectra for 250R1 in pure POPC bilayers were identical to those shown in Figure 10C. Although qualitatively similar to DM, there is an increase in the immobilized population in the lipid bilayers relative to DM at both pH values, likely due in part to the presence of **MI**, which is expected to more closely resemble **R** with an immobilized 250R1 (*64*). For 250R1 in bilayers of PC:PE:PS, $K = 4$ at pH 6 and $K = 1$ at pH 8, with corresponding **MI** populations of 30% and 50%, respectively. In addition, the detailed dynamics of the $\mathbf{MII_a}$ and $\mathbf{MII_b}$ substates, and hence the corresponding EPR spectra, could be different in bilayers and DM micelles, just as the dynamics of rhodopsin itself are different in these two environments.

***R* and *R**** *in Digitonin.* Digitonin is unique among micelle-forming amphiphiles in that the hydrophobic core of the micelle is essentially solid compared to the fluid interior of most micelles (*69*). Figure 11 shows the EPR spectra of **R** and **R*** for each of the sensor mutants in digitonin compared to DM and PC:PE:PS bilayers, each at pH 6. Overall, there is a striking immobilization of all R1 residues except for 316R1 in both **R** and **R*** in digitonin relative to DM.

For 140R1, the immobilization in digitonin is similar to that in lipid bilayers in both **R** and **R*** and likely has a similar origin, namely, direct contact with the solidlike interior of the digitonin micelle and with the highly ordered headgroup region of the bilayers, respectively (Figure 11A[1],[2]). As for the bilayer environment, there is no change upon activation to **R*** (Figure 11A[3]). For 227R1, there is a progressive decrease in overall mobility in the order DM > lipid bilayers > digitonin in both **R** and **R*** (Figure 11B[1],[2]), consistent with the view that this residue directly senses the hydrophobic interior of the respective structures.

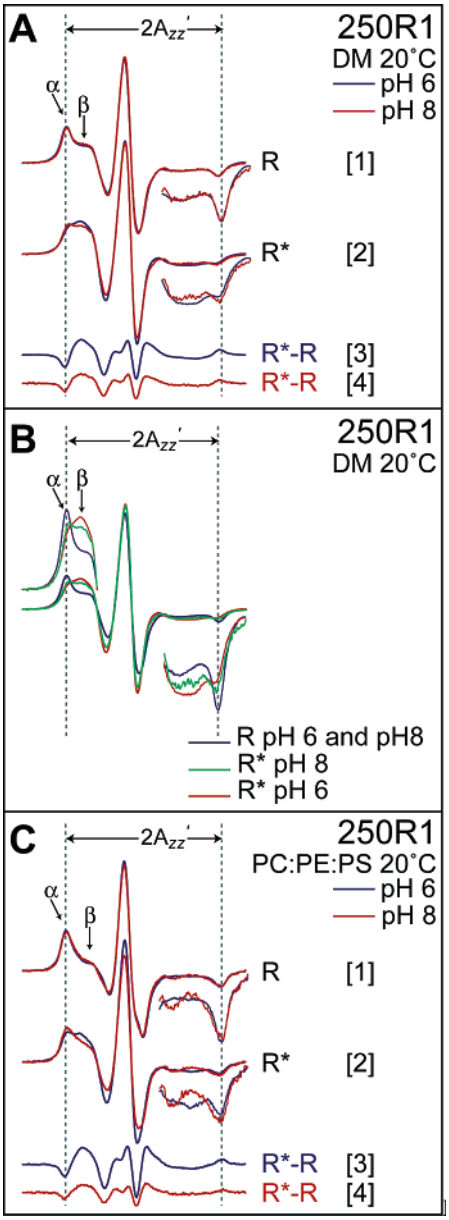


FIGURE 10: pH dependence of the EPR spectra of 250R1 in DM and PC:PE:PS bilayers at 20 °C. (A) Spectra for the indicated samples in DM (parts [1] and [2]). (B) Direct comparison of the spectra for **R** and **R*** in DM at pH 6 and 8. (C) Spectra for the corresponding samples in PC:PE:PS bilayers (parts [1] and [2]). In (A) and (C), **R*** − **R** difference spectra are shown to highlight the changes upon light activation at pH 6 and 8 (parts [3] and [4]). The insets for the EPR spectra show more clearly the differences in the low and high fields.

As for 140R1 in digitonin, there is no change in the EPR spectrum upon activation at 227R1 (Figure 11B[3]).

The EPR spectra of 250R1 **R** in digitonin and PC:PE:PS bilayers are similar (Figure 11C[1]), both showing a suppression of the more mobile population relative to DM. A dramatic difference is seen between 250R1 **R*** in digitonin micelles and in DM or lipid bilayers; digitonin effectively blocks the large increase in mobility of R1 and presumably the activating movement of TM6, seen in either of the other two environments (Figure 11C[2],[3]). Nevertheless, in digitonin 250R1 **R*** consists of approximately 20% **MI** and 80% $\mathbf{MII_a}$ at 20 °C, as determined by our visible absorbance spectra of the 250R1 mutant, which is consistent with the

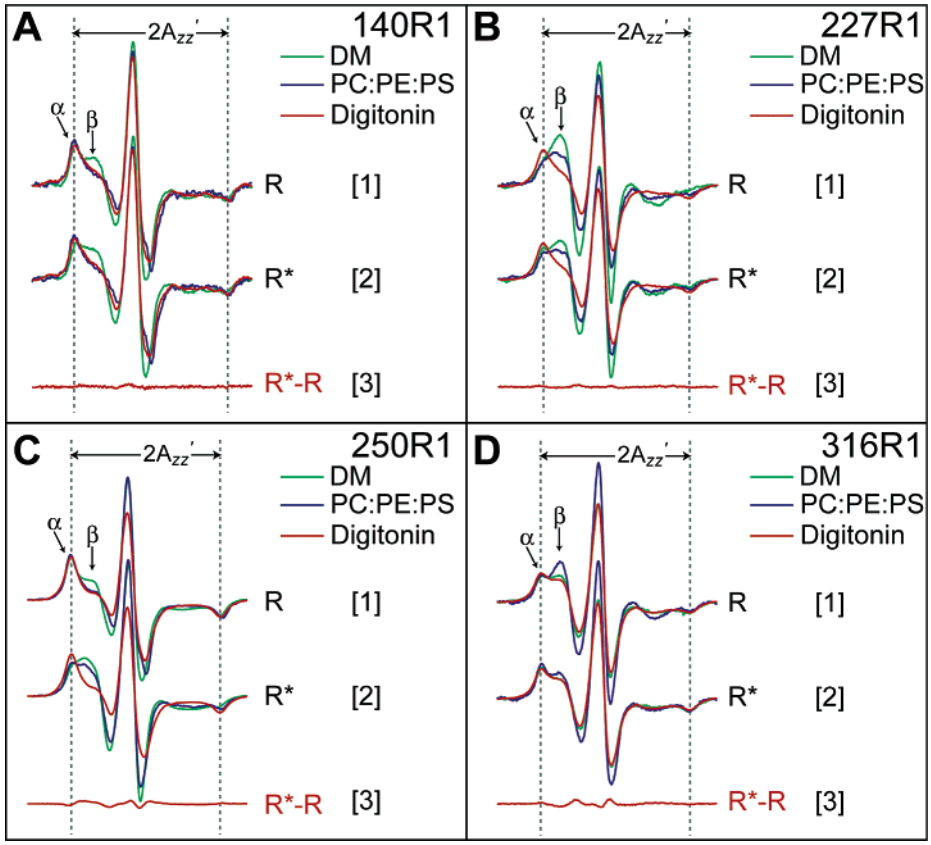


FIGURE 11: EPR spectra of 140R1, 227R1, 250R1, and 316R1 in digitonin (red) compared with those in DM (green) and PC:PE:PS bilayers (blue). In (A)−(D), spectra of the indicated spin-labeled mutant in **R** and **R*** are compared for the micellar and bilayer hosts. The **R*** − **R** difference spectrum in digitonin is shown in part [3].

analysis of Szundi et al. on WT rhodopsin (*23*). This result shows that the movement of TM6 at the cytoplasmic surface detected by 250R1 can be uncoupled from the deprotonation of the K296 Schiff base that accompanies the formation of **MII$_a$**. Unlike the other sites, the spectra of 316R1 are qualitatively similar in DM and digitonin both in **R** and in **R***, although the change upon light activation is much smaller in digitonin (Figure 11D).

## DISCUSSION

In previous studies of rhodopsin activation in DM micelles, EPR spectral changes of 227R1 and 250R1 were qualitatively interpreted in terms an outward tilt of TM6, while changes at 140R1 and 316R1 were taken to reflect unspecified structural rearrangements around TM3 and helix H8, respectively (*26*, *63*). The data presented here demonstrate a remarkable similarity of the activating conformational change of rhodopsin in DM micelles and phospholipid bilayers of pure POPC or POPC:POPE:POPS, as detected by 227R1, 250R1, and 316R1. Thus, the conclusions drawn from the extensive SDSL studies of rhodopsin in DM solutions (*26*) are generally expected to apply to the protein in a membrane environment.

The availability of a crystal structure for rhodopsin and structures for rotamers of the R1 side chain in helical proteins makes it possible to objectively model the spin-labeled proteins as a basis for a more quantitative interpretation of the EPR spectra and their changes upon activation in terms of protein structure and dynamics. As shown in the models of Figures 6 and 7, both 140R1 and 227R1 are in direct contact with the micelle or bilayer structures, and the motion of R1 is determined by the properties of the host system as well as the conformation of the protein. This situation complicates interpretation of the spectra in terms of protein conformation. As discussed above for 140R1, the strong immobilization of R1 in bilayers relative to DM could mean a change in structure but may also be due to its location in the highly ordered headgroup region of the bilayer. Under any circumstance, the immobilization renders 140R1 insensitive to change and of little use in exploring protein conformational states in rhodopsin in a bilayer environment. Residue 227R1 lies further toward the axial center of the protein, below the headgroup region, and senses properties of the hydrophobic domain of the host micelle or bilayer (Figures 7 and 11). Despite a damped motion in the bilayer's environment relative to DM, 227R1 still reports a change upon activation similar to, but smaller than, that seen in DM.

Unlike 140R1 and 227R1, 250R1 and 316R1 have no direct contacts with the host structure and reflect the conformation of the protein through tertiary contacts. Most important is 250R1 for which specific interpretations of the spectra in terms of structure can be given. Residue 250R1 fits in an existing pocket in the helix bundle and is not expected to produce significant structural perturbations (Figure 8C). The enhanced population of **MII** for 250R1 in bilayers ($K = 4$) relative to the WT protein ($K = 1.5$) at pH 6 corresponds to a free energy shift of only 0.6 kcal, possibly due to the strain energy of the nonrelaxed rotamer of R1 modeled in **R**.

Spectral simulations of 250R1 for **R** in DM and bilayers show the presence of comparable populations of both mobile and immobile states of the side chain (Figure 8B) in slow exchange on the EPR time scale (exchange rate $<10^7$ $s^{-1}$). The dynamic parameters of the mobile state indicate a relatively unconstrained motion (Table 1), similar to R1 on the exposed surface of a helix or loop structure, whereas modeling in the crystal structure of **R** suggests only a single highly constrained rotamer of the side chain that is expected to be immobilized (Figure 8C). This situation implies the existence of a second conformational substate, not observed in the confines of the crystal lattice, in which TM6 is partially displaced to remove constraints on R1 or in which there is partial unfolding of the cytoplasmic termination of TM6. The latter view is consistent with the previously characterized high flexibility of the TM5−TM6 loop that includes residues close to 250 (*63*, *70*). In this model, the cytoplasmic end of TM6 "flickers" between the two states.

For 250R1 in **R*** in both DM and bilayers, two dynamic populations of R1 are also observed, but with a population shift toward the more mobile state compared to **R**. However, the two states are not identical to the corresponding populations in **R**, and the transition to the activated state is not simply a shift in population between preexisting states. For the more immobile component in particular, the correlation times in **R*** are shorter than those in **R**. In one model for the conformational substates in **R***, the immobile state of R1 corresponds to a structure with TM6 in an **R**-like conformation but where the helix bundle has an increased "flexibility" reflected in the shorter correlation times. The substate giving rise to the mobile component corresponds to the previously identified state with TM6 tilted out (*30*, *63*). The notion of multiple conformational substates in rhodopsin based upon 250R1 is compatible with the two dynamic states of R1 seen at 140R1 in DM and 316R1 in DM and lipid bilayers, although modeling shows that the states could also arise from two rotamers of the side chain (Figures 6 and 9).

Although the conformations of **R** and **R*** are qualitatively similar in DM and phospholipid bilayers, there are interesting differences. For example, the shift in population toward a substate corresponding to the immobile state of 250R1 in lipid bilayers relative to DM (Figure 8) may be rationalized in terms of protein compressibility that arises from the existence of multiple conformations of different volumes in equilibrium. For example, a greater interfacial tension between the protein and lipids of the bilayer could effectively compress the protein and stabilize the lower volume state (*71*), presumed to correspond to the immobile population of 250R1. The extreme effect of digitonin on **R*** (Figure 11) that uncouples Schiff base deprotonation and TM6 movement and locks the conformation in an **R**-like state could arise from a similar effect. This model has been previously invoked to explain the influence of lipids (*72*, *73*) and detergents (*20*) on the optically detected conformational states of rhodopsin.

In DM, the $\mathbf{MII_a}$ and $\mathbf{MII_b}$ states can be differentially populated at pH 8 and 6, respectively (*20*). Assuming that the EPR spectra at pH 8 and 6 correspond to these intermediates, they are each composed of conformational substates (Figure 10), but $\mathbf{MII_b}$ has enhanced population of the mobile state, i.e., a substate with outward-tilted TM6. The similarity of the EPR spectra for **R*** in lipid bilayers and DM strongly supports the existence of similar states in lipid bilayers as well. In view of the above, it may be concluded that overall constraints on the motion of 250R1 are successively removed in passing from $\mathbf{R} > \mathbf{MII_a} > \mathbf{MII_b}$, suggesting that the molecule moves toward an increasingly open state.

Like 250R1, residue 316R1 provides a useful monitor of protein conformation free from direct effects of the host environment, but it is not yet possible to provide an unambiguous interpretation of the EPR spectra in terms of specific structures. Nevertheless, it can be concluded that the simple change in populations between mobile and immobile states upon photoactivation does not correspond to the extreme helix−coil transition proposed in one model for structural changes in helix H8 (*74*).

The identical behavior of **R*** in POPC:POPE:POPS and pure POPC bilayers should not be taken as inconsistent with the abundant evidence that the $\mathbf{MI} \leftrightarrows \mathbf{MII}$ equilibrium of photoactivated rhodopsin in bilayers, detected optically, is coupled to lipid composition (*57*, *72*, *73*). For example, the data presented above show that optical and structural transitions are not necessarily tightly coupled, and structural changes may not parallel changes in absorbance. Nevertheless, protein structural changes are expected to accompany changes in bilayer composition due to changes in hydrophobic mismatch (*75*), curvature stress (*76*), nonspecific electrostatic effects (*77*), or specific headgroup interactions (*78*).

In the present study, bilayer compositions and experimental conditions were selected to isolate effects due to specific headgroup interactions with the protein. The palmitoyl−oleoyl chain lengths provide a good match of the hydrophobic domains of the bilayers and protein (*79*) (Figure 2); any mismatch present is constant in the two bilayer systems studied. For POPC:POPE mixtures containing more than 39% POPC, hexagonal II ($H_{II}$) phases are not formed even in the presence of 20% dodecane (*80*), suggesting that the spontaneous curvature of the mixture used here with 50% POPC is relatively small. Thus, effects on protein conformation due to differences in curvature stress between the two bilayer compositions are also expected to be small.

The ionizable groups on PS and PE in mixed bilayers were previously shown to be fully charged throughout the pH range of 6−8 (*81*). All experiments reported here were carried out in 0.1 M ionic strength to reduce additional effects of the membrane double layer potential on surface pH in the PC:PE:PS bilayers. Tsui et al. measured the surface potentials of both reconstituted and native disk membranes, and the results suggest that at 0.1 M ionic strength the surface potential would not exceed ∼−25 mV for the PC:PE:PS reconstituted membranes, corresponding to a maximum pH decrease of ∼−0.4 unit at the surface relative to pure PC (*81*). Given the relatively small EPR spectral changes from pH 6 to pH 8 (Figure 10), the effect of surface pH difference between the bilayer systems would be very small.

The fact that identical EPR data were obtained for 140R1, 227R1, 250R1, and 316R1 in the two bilayer systems is thus interpreted as a lack of specific headgroup interactions that influence rhodopsin conformation in the regions sampled by these nitroxide sensors. Similar studies involving unsaturated lipids expected to have significant curvature stress are an

area for future investigation. In this regard, the helix tilt of rhodopsin, which changes the protein cross section differentially at the surface and bilayer interior, is an ideal model for testing curvature stress theories of protein−lipid interaction.

## ACKNOWLEDGMENT

We thank Dr. Nan-Jun Yu and Dr. Kewen Cai for contributions in the early phases of this work and Rob W. Herman for technical assistance.

## REFERENCES

1. Gether, U. (2000) Uncovering molecular mechanisms involved in activation of G protein-coupled receptors, *Endocr. Rev. 21*, 90−113.
2. Palczewski, K., Kumasaka, T., Hori, T., Behnke, C. A., Motoshima, H., Fox, B. A., Le Trong, I., Teller, D. C., Okada, T., Stenkamp, R. E., Yamanoto, M., and Miyano, M. (2000) Crystal structure of rhodopsin: a G protein-coupled receptor, *Science 289*, 739−745.
3. Teller, D. C., Okada, T., Behnke, C. A., Palczewski, K., and Stenkamp, R. E. (2001) Advances in determination of a high-resolution three-dimensional structure of rhodopsin, a model of G protein-coupled receptors (GPCRs), *Biochemistry 40*, 7761−7772.
4. Okada, T., Fujiyoshi, Y., Silow, M., Navarro, J., Landau, E. M., and Shichida, Y. (2002) Functional role of internal water molecules in rhodopsin revealed by X-ray crystallography, *Proc. Natl. Acad. Sci. U.S.A. 99*, 5982−5987.
5. Li, J., Edwards, P. C., Burghammer, M., Villa, C., and Schertler, G. F. (2004) Structure of bovine rhodopsin in a trigonal crystal form, *J. Mol. Biol. 343*, 1409−1438.
6. Lewis, J. W., and Kliger, D. S. (1992) Photointermediates of visual pigments, *J. Bioenerg. Biomembr. 24*, 201−210.
7. Melia, T. J., Cowan, C. W., Angleson, J. K., and Wensel, T. G. (1997) A comparison of the efficiency of G protein activation by ligand-free and light-activated forms of rhodopsin, *Biophys. J. 73*, 3182−3191.
8. Rao, V. R., and Oprian, D. D. (1996) Activating mutations of rhodopsin and other G protein-coupled receptors, *Annu. Rev. Biophys. Biomol. Struct. 25*, 287−314.
9. Vogel, R., and Siebert, F. (2001) Conformations of the active and inactive states of opsin, *J. Biol. Chem. 276*, 38487−38493.
10. Schoenlein, R. W., Peteanu, L. A., Mathies, R. A., and Shank, C. V. (1991) The first step in vision: femtosecond isomerization of rhodopsin, *Science 254*, 412−415.
11. Emeis, D., Kühn, H., Reichert, J., and Hofmann, K. P. (1982) Complex formation between metarhodopsin II and the GTP-binding protein in bovine photoreceptor membranes leads to a shift of the photoproduct equilibrium, *FEBS Lett. 143*, 29−34.
12. Heck, M., Schädel, S. A., Maretzki, D., Bartl, F., Ritter, E., Palczewski, K., and Hofmann, K. P. (2003) Signaling states of rhodopsin: formation of the storage form, metarhodopsin III, from active metarhodopsin II, *J. Biol. Chem. 278*, 3162−3169.
13. Longstaff, C., Calhoon, R. D., and Rando, R. R. (1986) Deprotonation of the Schiff base of rhodopsin is obligate in the activation of the G protein, *Proc. Natl. Acad. Sci. U.S.A. 83*, 4209−4213.
14. Sakmar, T. P., Franke, R. R., and Khorana, H. G. (1989) Glutamic acid-113 serves as the retinylidene Schiff base counterion in bovine rhodopsin, *Proc. Natl. Acad. Sci. U.S.A. 86*, 8309−8313.
15. Zhukovsky, E. A., and Oprian, D. D. (1989) Effect of carboxylic acid side chains on the absorption of visual pigments, *Science 246*, 928−930.
16. Yan, E. C. Y., Kazmi, M. A., Ganim, Z., Hou, J. M., Pan, D., Chang, B. S. W., Sakmar, T. P., and Mathies, R. A. (2003) Retinal counterion switch in the photoactivation of the G protein-coupled receptor rhodopsin, *Proc. Natl. Acad. Sci. U.S.A. 100*, 9262−9267.
17. Kim, J. M., Altenbach, C., Kono, M., Oprian, D. D., Hubbell, W. L., and Khorana, H. G. (2004) Structural origins of constitutive activation in rhodopsin: role of the K296/E113 salt bridge, *Proc. Natl. Acad. Sci. U.S.A. 101*, 12508−12513.
18. König, B., Welte, W., and Hofmann, K. P. (1989) Photoactivation of rhodopsin and interactions with transducin in detergent micelles. Effect of "doping" with steroid molecules, *FEBS Lett. 257*, 163−166.
19. Resek, J. F., Farahbakhsh, Z. T., Hubbell, W. L., and Khorana, H. G. (1993) Formation of the meta II photointermediate is accompanied by conformational changes in the cytoplasmic surface of rhodopsin, *Biochemistry 32*, 12025−12032.
20. Arnis, S., and Hofmann, K. P. (1993) Two different forms of metarhodopsin II: Schiff base deprotonation precedes proton uptake and signaling, *Proc. Natl. Acad. Sci. U.S.A. 90*, 7849−7853.
21. Stewart, J. G., Baker, B. N., and Williams, T. P. (1977) Evidence for conformeric states of rhodopsin, *Biophys. Struct. Mech. 3*, 19−29.
22. Bubis, J. (1998) Effects of detergents and lipids on transducin photoactivation by rhodopsin, *Biol. Res. 31*, 59−71.
23. Szundi, I., Lewis, J. W., and Kliger, D. S. (2005) Effect of digitonin on the rhodopsin meta I-meta II equilibrium, *Photochem. Photobiol. 81*, 866−873.
24. Ruprecht, J. J., Mielke, T., Vogel, R., Villa, C., and Schertler, G. F. (2004) Electron crystallography reveals the structure of metarhodopsin I, *EMBO J. 23*, 3609−3620.
25. Hubbell, W. L., Cafiso, D. S., and Altenbach, C. (2000) Identifying conformational changes with site-directed spin labeling, *Nat. Struct. Biol. 7*, 735−739.
26. Hubbell, W. L., Altenbach, C., Hubbell, C. M., and Khorana, H. G. (2003) Rhodopsin structure, dynamics, and activation: a perspective from crystallography, site-directed spin labeling, sulfhydryl reactivity, and disulfide cross-linking, *Adv. Protein Chem. 63*, 243−290.
27. Vogel, R., and Siebert, F. (2003) Fourier transform IR spectroscopy study for new insights into molecular properties and activation mechanisms of visual pigment rhodopsin, *Biopolymers 73*, 133−148.
28. Klein-Seetharaman, J., Yanamala, N. V., Javeed, F., Reeves, P. J., Getmanova, E. V., Loewen, M. C., Schwalbe, H., and Khorana, H. G. (2004) Differential dynamics in the G-protein coupled receptor rhodopsin revealed by solution NMR, *Proc. Natl. Acad. Sci. U.S.A. 101*, 3409−3413.
29. Patel, A. B., Crocker, E., Eilers, M., Hirshfeld, A., Sheves, M., and Smith, S. O. (2004) Coupling of retinal isomerization to the activation of rhodopsin, *Proc. Natl. Acad. Sci. U.S.A. 101*, 10048−10053.
30. Farrens, D. L., Altenbach, C., Yang, K., Hubbell, W. L., and Khorana, H. G. (1996) Requirement of rigid-body motion of transmembrane helices for light activation of rhodopsin, *Science 274*, 768−770.
31. Janz, J. M., and Farrens, D. L. (2004) Rhodopsin activation exposes a key hydrophobic binding site for the transducin α-subunit C terminus, *J. Biol. Chem. 279*, 29767−29773.
32. Elling, C. E., Nielsen, S. M., and Schwartz, T. W. (1995) Conversion of antagonist-binding site to metal-ion site in the tachykinin NK-1 receptor, *Nature 374*, 74−77.
33. Kobilka, B. K. (2002) Agonist-induced conformational changes in the $\beta_2$ adrenergic receptor, *J. Pept. Res. 60*, 317−321.
34. Knudsen, P., and Hubbell, W. L. (1978) Stability of rhodopsin in detergent solutions, *Membr. Biochem. 1*, 297−322.
35. Ramon, E., Marron, J., del Valle, L., Bosch, L., Andrés, A., Manyosa, J., and Garriga, P. (2003) Effect of dodecyl maltoside detergent on rhodopsin stability and function, *Vision Res. 43*, 3055−3061.
36. Kim, J. M., Altenbach, C., Thurmond, R. L., Khorana, H. G., and Hubbell, W. L. (1997) Structure and function in rhodopsin: rhodopsin mutants with a neutral amino acid at E134 have a partially activated conformation in the dark state, *Proc. Natl. Acad. Sci. U.S.A. 94*, 14273−14278.
37. Krebs, A., Edwards, P. C., Villa, C., Li, J., and Schertler, G. F. (2003) The three-dimensional structure of bovine rhodopsin determined by electron cryomicroscopy, *J. Biol. Chem. 278*, 50217−50225.
38. Oprian, D. D., Molday, R. S., Kaufman, R. J., and Khorana, H. G. (1987) Expression of a synthetic bovine rhodopsin gene in monkey kidney cells, *Proc. Natl. Acad. Sci. U.S.A. 84*, 8874−8878.
39. Robinson, P. R. (2000) Assays for detection of constitutively active opsin, *Methods Enzymol. 315*, 207−218.
40. Paternostre, M. T., Roux, M., and Rigaud, J. L. (1988) Mechanisms of membrane protein insertion into liposomes during reconstitution procedures involving the use of detergents. 1. Solubilization of large unilamellar liposomes (prepared by reverse-phase evaporation) by Triton X-100, octyl glucoside, and sodium cholate, *Biochemistry 27*, 2668−2677.

41. Rigaud, J. L., Pitard, B., and Levy, D. (1995) Reconstitution of membrane proteins into liposomes: application to energy-transducing membrane proteins, *Biochim. Biophys. Acta 1231*, 223−246.
42. Niu, L., Kim, J. M., and Khorana, H. G. (2002) Structure and function in rhodopsin: asymmetric reconstitution of rhodopsin in liposomes, *Proc. Natl. Acad. Sci. U.S.A. 99*, 13409−13412.
43. Hong, K., and Hubbell, W. L. (1972) Preparation and properties of phospholipid bilayers containing rhodopsin, *Proc. Natl. Acad. Sci. U.S.A. 69*, 2617−2621.
44. Bartlett, G. R. (1959) Phosphorous assay in column chromatography, *J. Biol. Chem. 234*, 466−468.
45. Mangold, H. K. (1967) Aliphatic lipids, in *Thin-layer Chromatography* (Stahl, E., Ed.) pp 363−415, Springer-Verlag, Berlin and New York.
46. Bhattacharya, S., Ridge, K. D., Knox, B. E., and Khorana, H. G. (1992) Light-stable rhodopsin. I. A rhodopsin analog reconstituted with a nonisomerizable 11-*cis* retinal derivative, *J. Biol. Chem. 267*, 6763−6769.
47. Columbus, L., Kálai, T., Jekö, J., Hideg, K., and Hubbell, W. L. (2001) Molecular motion of spin labeled side chains in α-helices: analysis by variation of side chain structure, *Biochemistry 40*, 3828−3846.
48. Budil, D. E., Lee, S., Saxena, S., and Freed, J. H. (1996) Nonlinear-least-squares analysis of slow-motion EPR spectra in one and two dimensions using a modified Levenberg-Marquardt algorithm, *J. Magn. Reson. 120*, 155−189.
49. Freed, J. H. (1976) Theory of slow tumbling ESR spectra for nitroxides, in *Spin Labeling. Theory and Applications* (Berliner, L. J., Ed.) pp 53−132, Academic Press, New York.
50. Langen, R., Oh, K. J., Cascio, D., and Hubbell, W. L. (2000) Crystal structures of spin labeled T4 lysozyme mutants: implications for the interpretation of EPR spectra in terms of structure, *Biochemistry 39*, 8396−8405.
51. Liang, Z., Lou, Y., Freed, J. H., Columbus, L., and Hubbell, W. L. (2004) A multifrequency electron spin resonance study of T4 lysozyme dynamics using the slowly relaxing local structure model, *J. Phys. Chem. B 108*, 17649−17659.
52. Columbus, L., and Hubbell, W. L. (2004) Mapping backbone dynamics in solution with site-directed spin labeling: GCN5-58 bZip free and bound to DNA, *Biochemistry 43*, 7273−7287.
53. Lietzow, M. A., and Hubbell, W. L. (2004) Motion of spin label side chains in cellular retinol-binding protein: correlation with structure and nearest-neighbor interactions in an antiparallel β-sheet, *Biochemistry 43*, 3137−3151.
54. Lovell, S. C., Word, J. M., Richardson, J. S., and Richardson, D. C. (2000) The penultimate rotamer library, *Proteins 40*, 389−408.
55. Daemen, F. J. (1973) Vertebrate rod outer segment membranes, *Biochim. Biophys. Acta 300*, 255−288.
56. Gibson, N. J., and Brown, M. F. (1993) Lipid headgroup and acyl chain composition modulate the MI-MII equilibrium of rhodopsin in recombinant membranes, *Biochemistry 32*, 2438−2454.
57. Botelho, A. V., Gibson, N. J., Thurmond, R. L., Wang, Y., and Brown, M. F. (2002) Conformational energetics of rhodopsin modulated by nonlamellar-forming lipids, *Biochemistry 41*, 6354−6368.
58. Isas, J. M., Langen, R., Hubbell, W. L., and Haigler, H. T. (2004) Structure and dynamics of a helical hairpin that mediates calcium-dependent membrane binding of annexin B12, *J. Biol. Chem. 279*, 32492−32498.
59. Chabre, M., and le Maire, M. (2005) Monomeric G-protein-coupled receptor as a functional unit, *Biochemistry 44*, 9395−9403.
60. Liang, Y., Fotiadis, D., Filipek, S., Saperstein, D. A., Palczewski, K., and Engel, A. (2003) Organization of the G protein-coupled receptor rhodopsin and opsin in membranes, *J. Biol. Chem. 278*, 21655−21662.
61. Jastrzebska, B., Maeda, T., Zhu, L., Fotiadis, D., Filipek, S., Engel, A., Stenkamp, R. E., and Palczewski, K. (2004) Functional characterization of rhodopsin monomers and dimers in detergents, *J. Biol. Chem. 279*, 54663−54675.
62. Filipek, S., Krzysko, K., Fotiadis, D., Liang, J., Saperstein, D. A., Engel, A., and Palczewski, K. (2004) A concept for G-protein activation by G protein-coupled receptor dimers: the transducin/rhodopsin interface, *Photochem. Photobiol. Sci. 3*, 628−638.
63. Altenbach, C., Yang, K., Farrens, D. L., Farahbakhsh, Z. T., Khorana, H. G., and Hubbell, W. L. (1996) Structural features and light-dependent changes in the cytoplasmic interhelical E-F loop region of rhodopsin: a site-directed spin-labeling study, *Biochemistry 35*, 12470−12478.
64. Schertler, G. F. (2005) Structure of rhodopsin and the meta-rhodopsin I photointermediate, *Curr. Opin. Struct. Biol. 15*, 408−415.
65. Medina, R., Perdomo, D., and Bubis, J. (2004) The hydrodynamic properties of dark- and light-activated states of *n*-dodecyl-β-D-maltoside-solubilized bovine rhodopsin support the dimeric structure of both conformations, *J. Biol. Chem. 279*, 39565−39573.
66. Baroin, A., Thomas, D. D., Osborne, B., and Devaux, P. F. (1977) Saturation transfer electron paramagnetic resonance on membrane-bound proteins. I. Rotational diffusion of rhodopsin in the visual receptor membrane, *Biochem. Biophys. Res. Commun. 78*, 442−447.
67. Kusumi, A., and Hyde, J. S. (1982) Spin-label saturation-transfer electron spin resonance detection of transient association of rhodopsin in reconstituted membranes, *Biochemistry 21*, 5978−5983.
68. Mchaourab, H. S., Lietzow, M. A., Hideg, K., and Hubbell, W. L. (1996) Motion of spin-labeled side chains in T4 lysozyme. Correlation with protein structure and dynamics, *Biochemistry 35*, 7692−7704.
69. Hong, K., and Hubbell, W. L. (1973) Lipid requirements for rhodopsin regenerability, *Biochemistry 12*, 4517−4523.
70. Columbus, L., and Hubbell, W. L. (2002) A new spin on protein dynamics, *Trends Biochem. Sci. 27*, 288−295.
71. Dan, A., and Safran, S. A. (1998) Effect of lipid characteristics on the structure of transmembrane proteins, *Biophys. J. 75*, 1410−1414.
72. Baldwin, P. A., and Hubbell, W. L. (1985) Effects of lipid environment on the light-induced conformational changes of rhodopsin. 2. Roles of lipid chain length, unsaturation, and phase state, *Biochemistry 24*, 2633−2639.
73. Brown, M. F. (1994) Modulation of rhodopsin function by properties of the membrane bilayer, *Chem. Phys. Lipids 73*, 159−180.
74. Krishna, A. G., Menon, S. T., Terry, T. J., and Sakmar, T. P. (2002) Evidence that helix 8 of rhodopsin acts as a membrane-dependent conformational switch, *Biochemistry 41*, 8298−8309.
75. Mouritsen, O. G., and Bloom, M. (1984) Mattress model lipid-protein interactions in membranes, *Biophys. J. 46*, 141−153.
76. Gruner, S. M. (1985) Intrinsic curvature hypothesis for biomembrane lipid composition: a role for nonbilayer lipids, *Proc. Natl. Acad. Sci. U.S.A. 82*, 3665−3669.
77. Gibson, N. J., and Brown, M. F. (1991) Role of phosphatidylserine in the MI-MII equilibrium of rhodopsin, *Biochem. Biophys. Res. Commun. 176*, 915−921.
78. Hessel, E., Heck, M., Muller, P., Herrmann, A., and Hofmann, K. P. (2003) Signal transduction in the visual cascade involves specific lipid-protein interactions, *J. Biol. Chem. 278*, 22853−22860.
79. Rappolt, M., Laggner, P., and Pabst, G. (2004) Structure and elasticity of phospholipid bilayers in the $L_\alpha$ phase: A comparison of phosphatidylcholine and phosphatidylethanolamine membranes, *Recent Res. Dev. Biophys. 3*, 363−392.
80. Lafleur, M., Cullis, P. R., Fine, B., and Bloom, M. (1990) Comparison of the orientational order of lipid chains in the $L_\alpha$ and $H_{II}$ phases, *Biochemistry 29*, 8325−8333.
81. Tsui, F. C., Ojcius, D. M., and Hubbell, W. L. (1986) The intrinsic p$K_a$ values for phosphatidylserine and phosphatidylethanolamine in phosphatidylcholine host bilayers, *Biophys. J. 49*, 459−468.

BI060101V